



Search for the $\Lambda_b^0 \rightarrow \Lambda\eta'$ and $\Lambda_b^0 \rightarrow \Lambda\eta$ decays with the LHCb detector

The LHCb collaboration[†]

Abstract

A search is performed for the as yet unobserved baryonic $\Lambda_b^0 \rightarrow \Lambda\eta'$ and $\Lambda_b^0 \rightarrow \Lambda\eta$ decays with 3 fb^{-1} of proton-proton collision data recorded by the LHCb experiment. The $B^0 \rightarrow K_s^0\eta'$ decay is used as a normalisation channel. No significant signal is observed for the $\Lambda_b^0 \rightarrow \Lambda\eta'$ decay. An upper limit is found on the branching fraction of $\mathcal{B}(\Lambda_b^0 \rightarrow \Lambda\eta') < 3.1 \times 10^{-6}$ at 90% confidence level. Evidence is seen for the presence of the $\Lambda_b^0 \rightarrow \Lambda\eta$ decay at the level of 3σ significance, with a branching fraction $\mathcal{B}(\Lambda_b^0 \rightarrow \Lambda\eta) = (9.3^{+7.3}_{-5.3}) \times 10^{-6}$.

Published as JHEP 09 (2015) 006

© CERN on behalf of the LHCb collaboration, licence CC-BY-4.0.

[†]Authors are listed at the end of this paper.

1 Introduction

One of the interesting features of SU(3) flavour symmetry breaking in the light neutral meson sector is the mixing of singlet and octet states in the pseudoscalar mesons. The physical η and η' particles can be expressed as an admixture of light quark and strange quark flavour eigenstates [1],

$$\begin{pmatrix} |\eta\rangle \\ |\eta'\rangle \end{pmatrix} = \begin{pmatrix} \cos \phi_p & -\sin \phi_p \\ \sin \phi_p & \cos \phi_p \end{pmatrix} \begin{pmatrix} |\eta_q\rangle \\ |\eta_s\rangle \end{pmatrix}, \quad (1)$$

where the quark states are defined as

$$|\eta_q\rangle = \frac{1}{\sqrt{2}}|u\bar{u} + d\bar{d}\rangle \quad \text{and} \quad |\eta_s\rangle = |s\bar{s}\rangle, \quad (2)$$

and ϕ_p is the mixing angle between light and strange quark states. In principle all possible SU(3) flavour singlet states that contribute to the physical particles, including the gluonic wavefunction, $|gg\rangle$, and the heavier quarkonia wavefunctions, $|c\bar{c}\rangle$ and $|b\bar{b}\rangle$, must be considered. Of these states, only $|gg\rangle$ is considered to contribute to the mass eigenstates [2–4], and this only occurs in the heavier η' meson [1, 5]. Introducing the gluon mixing angle ϕ_G , the η' wavefunction becomes

$$|\eta'\rangle = \cos \phi_G \sin \phi_p |\eta_q\rangle + \cos \phi_G \cos \phi_p |\eta_s\rangle + \sin \phi_G |gg\rangle. \quad (3)$$

Many phenomenological and experimental studies have been carried out to determine the values of the mixing angles, and measurements are in the range $\phi_p \approx 38 - 46^\circ$ [6–17]. Refs. [15–17] also contain measurements of the gluonic mixing angle, which are consistent with zero, albeit with large uncertainties. Most recently, the mixing angles have been measured by the LHCb experiment using $B_{(s)}^0 \rightarrow J/\psi \eta^{(\prime)}$ decays, and are found to be $\phi_p = (43.5_{-2.8}^{+1.5})^\circ$ and $\phi_G = (0 \pm 25)^\circ$ [18].

One consequence of the mixing is the difference in branching fractions for b-hadron decays to final states containing η and η' mesons. The gluonic mixing alters the branching fraction for the decays to η' mesons compared with the equivalent decay to η mesons. Possible Feynman diagrams for amplitudes contributing to the $\Lambda_b^0 \rightarrow \Lambda \eta^{(\prime)}$ decays are shown in Fig. 1, with Fig. 1(a) showing the dominant $b \rightarrow s$ transition via a penguin diagram. Due to the gluonic contribution of the wavefunction, extra Feynman diagrams of similar amplitude are available for the η' decay [19]. These include the possible non-spectator contribution, where the light quark radiates a gluon which can form an η' meson, as shown in Fig. 1(b), and the anomalous contribution, where an excited gluon in the decay can radiate an η' meson, as shown in Fig. 1(c). The amplitudes for these extra processes can interfere to enhance or reduce the branching fraction to η' mesons. For example, the branching fraction for the $B^0 \rightarrow K^0 \eta'$ decay¹ has been measured to be $(6.6 \pm 0.4) \times 10^{-5}$ which is over 50 times larger than the branching fraction for the $B^0 \rightarrow K^0 \eta$ decay [20].

¹Charge-conjugation is implied throughout.

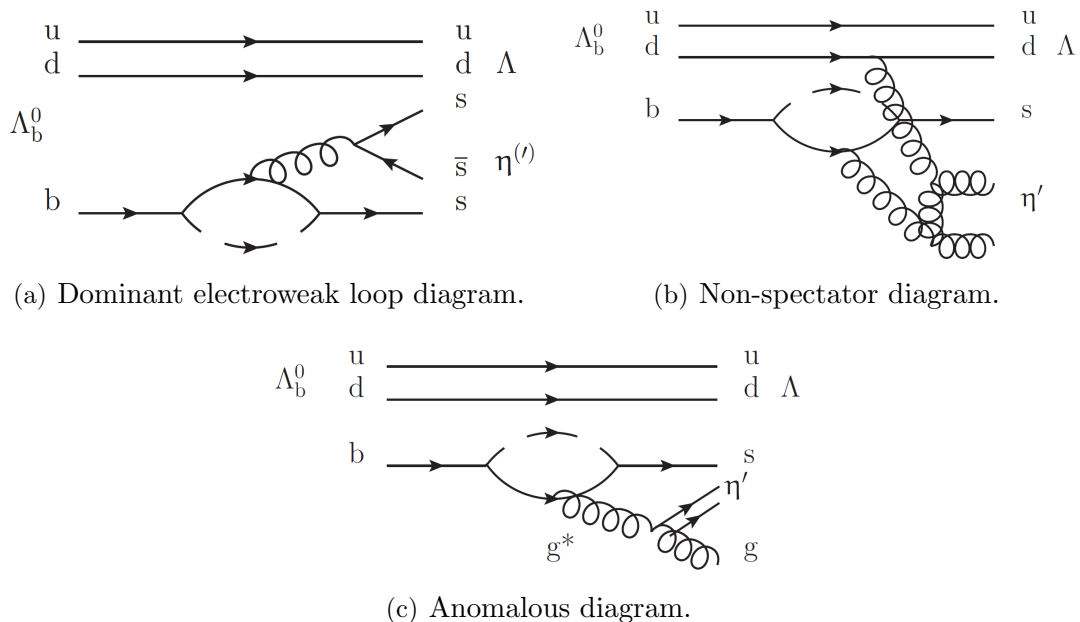


Figure 1: Feynman diagrams for the $\Lambda_b^0 \rightarrow \Lambda \eta^{(\prime)}$ decay. The non-spectator and anomalous diagrams are available only to the η' through the gluonic contribution.

By measuring the relative branching fractions of many different decays to final states containing η and η' mesons, it is possible to extract a measurement of the mixing angle ϕ_p . Decays of b-baryons to final states containing η or η' mesons have not yet been observed; however, the branching fractions of the Λ_b^0 decays have been estimated to be in the range $(1.8 - 19.0) \times 10^{-6}$ [21], depending on the model used to calculate the hadronic form factors. The interference between the anomalous and non-spectator contributions cancel in such a way that the branching fractions for the $\Lambda_b^0 \rightarrow \Lambda \eta'$ and $\Lambda_b^0 \rightarrow \Lambda \eta$ decays are expected to be similar. Using the QCD sum rules approach to calculate the hadronic form factors, the branching fractions are predicted to be in the range $(6.0 - 19.0) \times 10^{-6}$. The pole model approach predicts smaller branching fractions, in the range $(1.8 - 4.5) \times 10^{-6}$. For comparison, if the anomalous contribution is neglected, the branching fraction for the $\Lambda_b^0 \rightarrow \Lambda \eta'$ decay would increase to $(33 - 40) \times 10^{-6}$ [21].

This paper describes the search for the $\Lambda_b^0 \rightarrow \Lambda \eta'$ and $\Lambda_b^0 \rightarrow \Lambda \eta$ decays and measurement of the relative branching fractions with respect to the $B^0 \rightarrow K^0 \eta'$ decay, using the 3 fb^{-1} of data in pp collisions collected in 2011 and 2012 by the LHCb experiment.

2 LHCb detector, trigger and event simulation

The LHCb detector [22,23] is a single-arm forward spectrometer covering the pseudorapidity range $2 < \eta < 5$, designed for the study of particles containing b or c quarks. The detector

includes a high-precision tracking system consisting of a silicon-strip vertex detector surrounding the pp interaction region [24], a large-area silicon-strip detector located upstream of a dipole magnet with a bending power of about 4 Tm, and three stations of silicon-strip detectors and straw drift tubes [25] placed downstream of the magnet. The tracking system provides a measurement of momentum, p , of charged particles with a relative uncertainty that varies from 0.5% at low momentum to 1.0% at 200 GeV/ c . The minimum distance of a track to a primary vertex, the impact parameter, is measured with a resolution of $(15 + 29/p_T) \mu\text{m}$, where p_T is the component of the momentum transverse to the beam, in GeV/ c . Different types of charged hadrons are distinguished using information from two ring-imaging Cherenkov (RICH) detectors [26]. Photons, electrons and hadrons are identified by a calorimeter system consisting of scintillating-pad and preshower detectors, an electromagnetic calorimeter and a hadronic calorimeter. Muons are identified by a system composed of alternating layers of iron and multiwire proportional chambers [27].

The trigger [28] consists of a hardware stage, based on information from the calorimeter and muon systems, followed by a software stage, in which all charged particles with $p_T > 500$ (300) MeV/ c are reconstructed for 2011 (2012) data. The software trigger requires a two-, three- or four-track secondary vertex with a significant displacement from any primary pp interaction vertex (PV). At least one charged particle must have a transverse momentum $p_T > 1.7$ GeV/ c and be inconsistent with originating from a PV. A multivariate algorithm [29] is used for the identification of secondary vertices consistent with the decay of a b-hadron.

In the simulation, pp collisions are generated using PYTHIA [30] with a specific LHCb configuration [31]. Decays of hadronic particles are described by EVTGEN [32], in which final-state radiation is generated using PHOTOS [33]. The interaction of the generated particles with the detector, and its response, are implemented using the GEANT4 toolkit [34] as described in Ref. [35].

3 Event selection

Candidate signal events are identified by reconstructing the $\Lambda_b^0 \rightarrow \Lambda \eta'$ and $\Lambda_b^0 \rightarrow \Lambda \eta$ decays. The decay $B^0 \rightarrow K_s^0 \eta'$ is used as a normalisation channel for the measurement of the branching fractions of the signal decays.

The long-lived K_s^0 and Λ particles are reconstructed through the $K_s^0 \rightarrow \pi^+ \pi^-$ and $\Lambda \rightarrow p \pi^-$ decays. The reconstruction of these particles is labelled according to where in the LHCb detector the decay occurs. If the particle decay products produce hits in the vertex detector then the candidate is classified as *Long* (L); otherwise the candidate is referred to as *Downstream* (D). Since the track resolution is different for the two categories, the selection is optimised separately for L and D candidates.

The candidate η' mesons in the $\Lambda_b^0 \rightarrow \Lambda \eta'$ decay are reconstructed as $\eta' \rightarrow \pi^+ \pi^- \gamma$ and $\eta' \rightarrow \pi^+ \pi^- \eta$, where the η meson decays into two photons. The candidate η mesons used in the reconstruction of the $\Lambda_b^0 \rightarrow \Lambda \eta$ decay are reconstructed with the $\eta \rightarrow \pi^+ \pi^- \pi^0$ decay,

with the π^0 meson decaying into two photons. Since the charged tracks in the $\eta \rightarrow \pi^+\pi^-\pi^0$ decay can be used for the trigger selection, the analysis is based on this mode rather than the neutral decays of the η meson, which would have a lower efficiency.

Events that pass the trigger selection are subject to further requirements consisting of kinematic, particle identification and multivariate selections. A minimum requirement is placed on the fit quality of the reconstructed vertices. When reconstructing the B^0 and Λ_b^0 candidates, the direction angle² and the impact parameter are required to be consistent with the reconstructed particle originating from a PV, and the calculated lifetime should be significantly different from zero. The B^0 (Λ_b^0) candidates are required to have $p_T > 1.5$ (1.0) GeV/ c . The K_S^0 mesons are required to have $p_T > 1.2$ GeV/ c and a flight distance significantly different from zero. The invariant mass of the $\pi^+\pi^-$ pair should be within 14 MeV/ c^2 of the known K^0 mass [20] for events in the L category, and be within 23 MeV/ c^2 for events in the D category, where the mass window is chosen to be three times the resolution of the invariant mass. The Λ baryon should have $p_T > 1$ GeV/ c and an invariant mass within 15 MeV/ c^2 of the known Λ mass [20] for the L category, and within 20 MeV/ c^2 for the D category. The η' and η mesons from B^0 and Λ_b^0 decays are required to have $p_T > 2$ GeV/ c . Reconstructed $\pi^+\pi^-\gamma$ and $\pi^+\pi^-\eta$ candidates are required to have an invariant mass in the range [0.9,1.05] GeV/ c^2 and $\pi^+\pi^-\pi^0$ candidates should have an invariant mass in a 150 MeV/ c^2 window around the known η meson mass [20]. Charged tracks are required to be of good quality with $p_T > 300$ MeV/ c . The η mesons from η' decays, and π^0 mesons from η decays are reconstructed from two photons which can be resolved in the calorimeter, with an invariant mass in a 50 MeV/ c^2 window around the η or π^0 mass [20], and the η or π^0 mesons are required to have $p_T > 200$ MeV/ c . Finally, photons are required to have a transverse energy $E_T > 200$ MeV, and a large p-value for the single photon hypothesis, in order to reject background from misidentified π^0 mesons where both decay photons form a single merged cluster in the calorimeter.

To improve the resolution of the reconstructed invariant mass, the full decay chain is refitted, where the tracks and displaced vertices are constrained, with the position of the PV of the B^0 or Λ_b^0 candidate fixed to the PV refitted using only tracks not associated to the b-hadron decays, and the invariant mass of the K_S^0 , Λ , η' and η particles fixed to their known masses [36]. Candidates with a poor quality in this constrained fit are rejected, which removes approximately 90% of background from the L category and 20% of the background from the D category.

Information from the RICH detectors and the LHCb calorimeter system is used in a neural network to construct a probability that a track is a pion, a kaon or a proton. This particle identification (PID) information is used to reduce the background from misidentified kaons, protons and pions.

A boosted decision tree (BDT) [37,38] is used to obtain further discrimination between signal and background events. A different BDT is trained for each signal channel and the normalisation channel, separately for the L and D categories and the 2011 and 2012 data samples. Samples of simulated events are used to model the signal decays, and events

²The direction angle is defined as the angle between the momentum vector of the particle and the vector between the PV and the decay vertex.

in data with a reconstructed invariant mass greater than $100 \text{ MeV}/c^2$ above the B^0 or Λ_b^0 mass [20] are used to model the combinatorial background.

In this analysis, the numbers of candidates in both the signal and the background samples are limited and the performance of the BDT is improved in two ways. In the simulated signal sample no requirements are placed on the trigger selection. Instead, the kinematic distributions of the candidates are reweighted in order to match the harder distributions of candidates which pass the trigger selection. In addition, the signal and background samples are split in two, and two BDTs are trained for each channel. The first half of the sample is used to train a BDT which is applied to the second half of the data, and vice versa for the second BDT. This way, all data are available in the training of the BDTs, while any bias in the multivariate selection is avoided.

The BDT uses a set of variables with discriminating power between signal and background, including kinematic variables and vertex and track quality variables, and combines them into one variable which separates signal and background well. The selection is optimised using the figure of merit $\epsilon_{\text{MVA}}/(\frac{a}{2} + \sqrt{N_{\text{B}}})$ [39], where ϵ_{MVA} is the selection efficiency for a particular BDT selection, $a = 3$ is the targeted signal significance in standard deviations, and N_{B} is the number of combinatorial background events reconstructed within the signal region and passing the BDT selection, found by performing an unbinned extended maximum likelihood fit to the sidebands of the data and extrapolating this fit into the signal region.

The final stage is to ensure that each event passing the selection contains exactly one B^0 or Λ_b^0 candidate. Due to the poor invariant mass resolution of the $\eta^{(\prime)}$ mesons, it is possible for low energy photons from the underlying event to be reconstructed with signal pions to create a second $\eta^{(\prime)}$ candidate. This happens in about 10% – 20% of events which pass the selection. In this situation the candidate with the highest E_{T} photon is kept, and all other candidates in the event are rejected.

The efficiency of this selection is $(0.032 \pm 0.001)\%$ in the L category and $(0.030 \pm 0.001)\%$ in the D category. This includes the efficiency of reconstructing and selecting events which are simulated within the LHCb detector acceptance.

4 Results

4.1 Fit results and signal yields

An unbinned extended maximum likelihood fit to the candidate b-hadron mass spectrum is performed on the data which pass the selection. The model used for the fit to both the signal and normalisation channels consists of an exponential function to describe the combinatorial background, and a sum of two Gaussian functions with a common mean to describe the signal. The ratio of the resolutions of the two Gaussian functions and the ratio of the signal yields are obtained from a fit to the mass distribution in simulated signal samples. These parameter values are used in the fit to the data, and only the resolution and signal yield of the first Gaussian function and, for the normalisation channel, the common mean of the two Gaussian functions are allowed to float. The resolution of the reconstructed

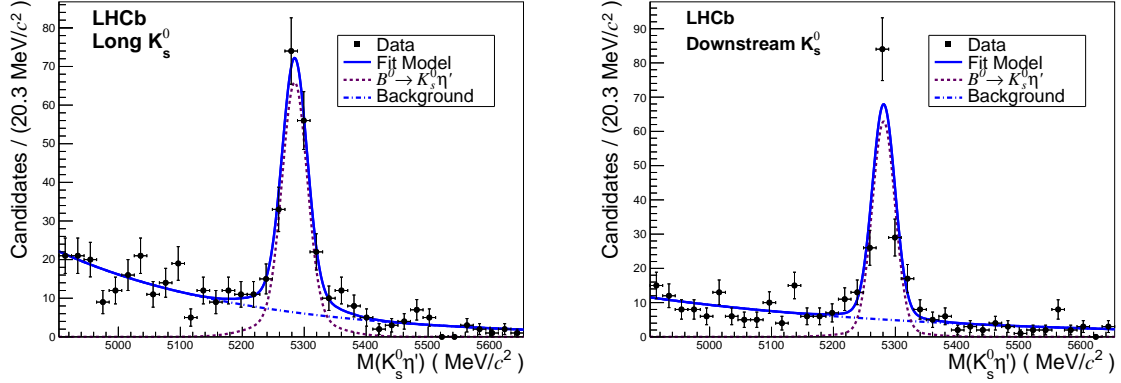


Figure 2: Mass distribution of the selected $B^0 \rightarrow K_s^0 \eta'$ ($\eta' \rightarrow \pi^+ \pi^- \gamma$) candidates in the 2011 and 2012 data, reconstructed in the L (left) and D (right) categories. The results of the fit, as described in the text, are overlaid.

$K_s^0 \eta'$ invariant mass is $30.0 \pm 1.5 \text{ MeV}/c^2$ for L candidates and $29.4 \pm 1.3 \text{ MeV}/c^2$ for D candidates. For the signal channels, the resolution of the reconstructed $\Lambda \eta'$ invariant mass is $29.1 \pm 1.8 \text{ MeV}/c^2$ ($31.1 \pm 4.5 \text{ MeV}/c^2$) for candidates reconstructed with $\eta' \rightarrow \pi^+ \pi^- \gamma$ in the $L(D)$ category, and $47.8 \pm 9.2 \text{ MeV}/c^2$ ($56.6 \pm 10.9 \text{ MeV}/c^2$) for candidates reconstructed with $\eta' \rightarrow \pi^+ \pi^- \eta$ in the $L(D)$ category. Reconstructed $\Lambda \eta$ candidates have an invariant mass resolution of $49.4 \pm 3.4 \text{ MeV}/c^2$ in the L category and $47.6 \pm 9.2 \text{ MeV}/c^2$ in the D category. The parameters of the fit are found to be consistent between the 2011 and 2012 data samples, and so the two samples are added together to perform an overall fit.

The possible presence of physics backgrounds has been investigated. The most likely backgrounds are: b-hadron decay modes to mesons with open charm and an $\eta^{(\prime)}$ meson, with a π^0 meson which is not reconstructed; the nonresonant decays to K_s^0 or Λ particles with two charged pions which are combined with a combinatorial photon, π^0 or η meson to form an $\eta^{(\prime)}$ meson candidate; or, in the case of the $\eta' \rightarrow \pi^+ \pi^- \gamma$ decays, the nonresonant $B^0 \rightarrow K_s^0 \pi^+ \pi^- \gamma$ or $\Lambda_b^0 \rightarrow \Lambda \pi^+ \pi^- \gamma$ decays. These backgrounds are rejected well by the BDT selection, and there are expected to be fewer than one candidate from each category passing the selection.

For the normalisation channel, the mass distribution of the selected $K_s^0 \eta'$ candidates is shown in Fig. 2, with the result of the fit superimposed. The signal yields are 188 ± 16 L candidates and 149 ± 14 D candidates, and the signal to background ratio is 1.8 in the L category, and 1.7 in the D category. Fig. 3 shows the invariant mass distribution of the reconstructed η' mesons for these decays. The distribution is fitted with two Crystal Ball functions [40], and the parameters are found to be consistent with fits to the simulated samples, with a core resolution of $16 \pm 6 \text{ MeV}/c^2$ for L candidates and $13 \pm 1 \text{ MeV}/c^2$ for D candidates.

For the signal channel, Fig. 4 shows the $\Lambda \eta'$ invariant mass distribution for candidates reconstructed in the $\Lambda_b^0 \rightarrow \Lambda \eta'$ ($\eta' \rightarrow \pi^+ \pi^- \gamma$) decay, while Fig. 5 shows the same distribution

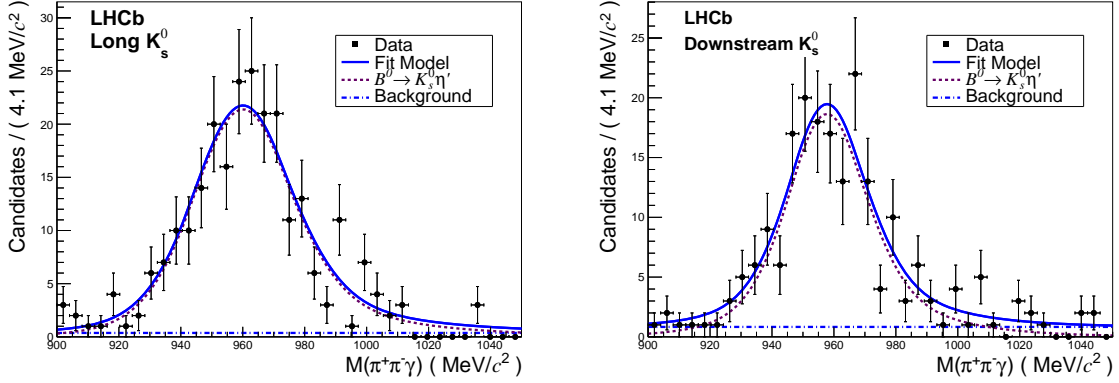


Figure 3: Mass distribution of the reconstructed η' meson for selected $B^0 \rightarrow K_s^0 \eta'$ ($\eta' \rightarrow \pi^+ \pi^- \gamma$) candidates, in the L (left) and D (right) categories. The results of the fit, as described in the text, are overlaid.

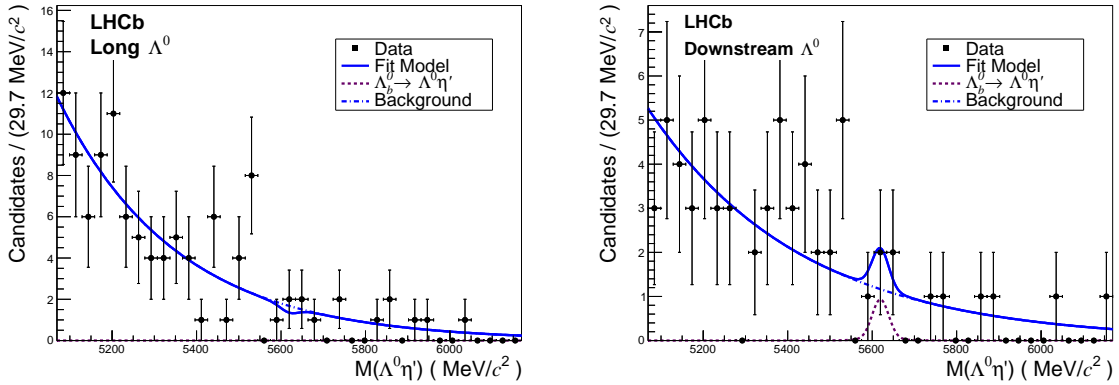


Figure 4: Mass distribution of the selected $\Lambda_b^0 \rightarrow \Lambda \eta'$ ($\eta' \rightarrow \pi^+ \pi^- \gamma$) candidates in the 2011 and 2012 data, reconstructed in the L (left) and D (right) categories. The results of the fit, as described in the text, are overlaid.

for candidates in the $\Lambda_b^0 \rightarrow \Lambda \eta'$ ($\eta' \rightarrow \pi^+ \pi^- \eta$) channel, and Fig. 6 shows the $\Lambda \eta$ invariant mass distribution for $\Lambda_b^0 \rightarrow \Lambda \eta$ ($\eta \rightarrow \pi^+ \pi^- \pi^0$) candidates. An unbinned extended maximum likelihood fit is performed using the same model as for the B^0 decay, with an exponential function to describe the combinatorial background and a sum of two Gaussian functions to model the signal; all parameters are fixed to the values found from fits to the simulation, and only the numbers of signal and background events are allowed to float in the fit. No significant signal is observed above the expected background for the $\Lambda_b^0 \rightarrow \Lambda \eta'$ channel, and so an upper limit is placed on the ratio of branching fractions. From the fits, the combined signal yields are 1.0 ± 4.4 $\Lambda_b^0 \rightarrow \Lambda \eta'$ ($\eta' \rightarrow \pi^+ \pi^- \gamma$) candidates and -4.2 ± 2.3

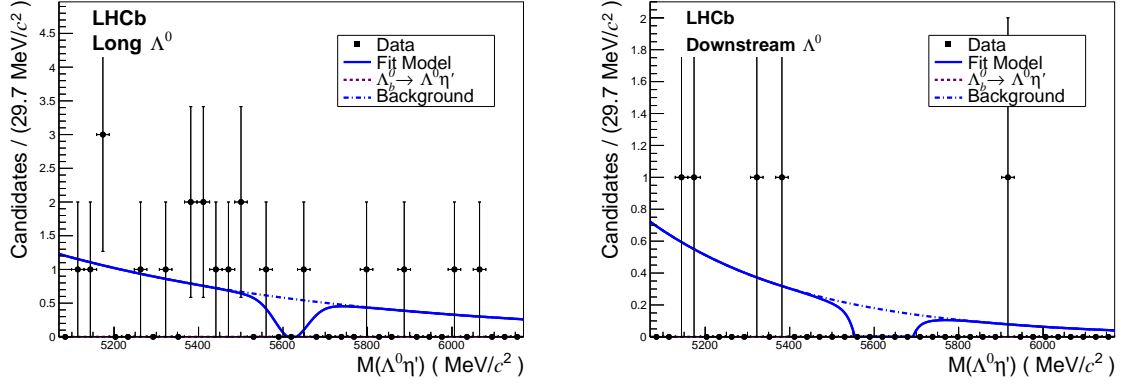


Figure 5: Mass distribution of the selected $\Lambda_b^0 \rightarrow \Lambda \eta'$ ($\eta' \rightarrow \pi^+ \pi^- \eta$) candidates in the 2011 and 2012 data, reconstructed in the L (left) and D (right) categories. The results of the fit, as described in the text, are overlaid.

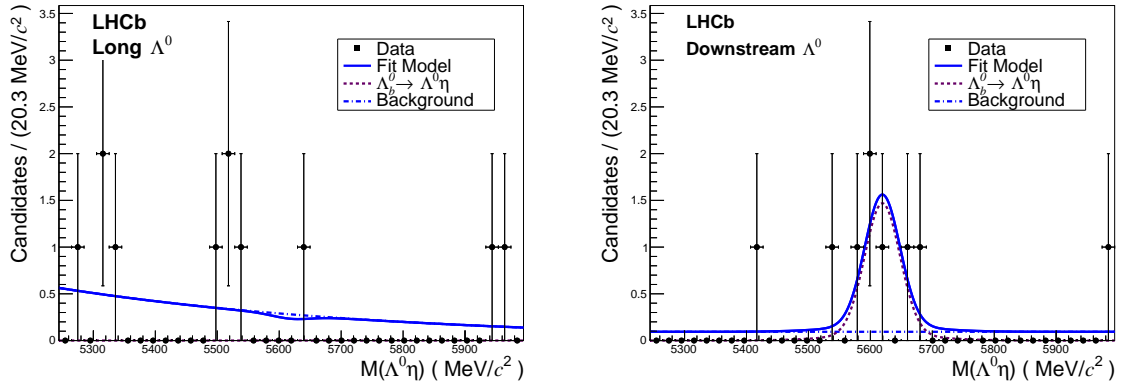


Figure 6: Mass distribution of the selected $\Lambda_b^0 \rightarrow \Lambda \eta$ ($\eta \rightarrow \pi^+ \pi^- \pi^0$) candidates in the 2011 and 2012 data, reconstructed in the L (left) and D (right) categories. The results of the fit, as described in the text, are overlaid.

$\Lambda_b^0 \rightarrow \Lambda \eta'$ ($\eta' \rightarrow \pi^+ \pi^- \eta$) candidates. Evidence is seen for the presence of the $\Lambda_b^0 \rightarrow \Lambda \eta$ decay with a signal yield of 5.3 ± 3.8 candidates, and a significance of 3.0σ .

Table 1: Components contributing to the scale factor α .

Factor	$\Lambda\eta'(\pi^+\pi^-\gamma)$		$\Lambda\eta'(\pi^+\pi^-\eta)$		$\Lambda\eta(\pi^+\pi^-\pi^0)$	
	L	D	L	D	L	D
$\epsilon_{\text{tot}}(\text{B}^0)/\epsilon_{\text{tot}}(\Lambda_{\text{b}}^0)$	2.3 ± 0.1	1.55 ± 0.08	7.4 ± 0.6	9.5 ± 1.4	4.6 ± 0.3	3.4 ± 0.2
$f_{\text{B}}/f_{\Lambda_{\text{b}}^0}$	2.5 ± 0.2		2.5 ± 0.2		2.5 ± 0.2	
$1/C_{\gamma}$	1 (fixed)		0.95 ± 0.04		1.13 ± 0.04	
$0.5 \cdot \mathcal{B}(\text{K}_{\text{s}}^0)/\mathcal{B}(\Lambda)$	0.541 ± 0.004		0.541 ± 0.004		0.541 ± 0.004	
$\mathcal{B}(\eta')/\mathcal{B}(\eta^{(\prime)})$	1 (fixed)		1.71 ± 0.05		1.31 ± 0.03	
α	3.1 ± 0.3	2.1 ± 0.2	17.7 ± 2.3	22.8 ± 4.0	9.5 ± 1.2	7.0 ± 0.8

4.2 Branching fraction measurement

The ratio of branching fractions can be measured for each signal decay with respect to the normalisation channel using

$$\begin{aligned}
 R &\equiv \frac{\mathcal{B}(\Lambda_{\text{b}}^0 \rightarrow \Lambda\eta^{(\prime)})}{\mathcal{B}(\text{B}^0 \rightarrow \text{K}^0\eta')} \\
 &= \frac{N_{\text{S}}(\Lambda_{\text{b}}^0)}{N_{\text{S}}(\text{B}^0)} \times \frac{\epsilon_{\text{tot}}(\text{B}^0)}{\epsilon_{\text{tot}}(\Lambda_{\text{b}}^0)} \times \frac{f_{\text{B}}}{f_{\Lambda_{\text{b}}^0}} \times \frac{1}{C_{\gamma}} \times \frac{\mathcal{B}(\eta')}{\mathcal{B}(\eta^{(\prime)})} \times \frac{0.5 \times \mathcal{B}(\text{K}^0)}{\mathcal{B}(\Lambda)} \\
 &= \alpha \times \frac{N_{\text{S}}(\Lambda_{\text{b}}^0)}{N_{\text{S}}(\text{B}^0)},
 \end{aligned} \tag{4}$$

where: N_{S} is the number of signal events determined from the fits to data; ϵ_{tot} is the total efficiency, which is the product of the detector acceptance, reconstruction and selection efficiencies; $f_{\text{B}}/f_{\Lambda_{\text{b}}^0}$ is the ratio of B^0 to Λ_{b}^0 production fractions, previously measured by LHCb [41]; $1/C_{\gamma}$ is a correction factor applied to account for the photon reconstruction efficiency in the $\Lambda_{\text{b}}^0 \rightarrow \Lambda\eta'$ ($\eta' \rightarrow \pi^+\pi^-\eta$) and $\Lambda_{\text{b}}^0 \rightarrow \Lambda\eta$ ($\eta \rightarrow \pi^+\pi^-\pi^0$) decays, which have more photons in the decay than the normalisation channel; and $\mathcal{B}(\eta')/\mathcal{B}(\eta^{(\prime)})$ and $\mathcal{B}(\text{K}_{\text{s}}^0)/\mathcal{B}(\Lambda)$ are the ratios of η' to $\eta^{(\prime)}$ branching fractions and K_{s}^0 to Λ branching fractions, respectively, from Ref. [20], where the factor 0.5 accounts for the fact that only half the K^0 mesons decay as K_{s}^0 mesons. Each of these factors have been measured, as described in Sec. 5, and are given in Table 1 along with the calculated value of α for each signal channel.

5 Systematic uncertainties

A summary of systematic uncertainties is given in Table 2. The largest systematic uncertainty for this analysis is due to the limited knowledge of the ratio of production fractions, $f_{\text{B}}/f_{\Lambda_{\text{b}}^0}$, which was measured in Ref. [41] as a function of the Λ_{b}^0 pseudorapidity.

Table 2: Fractional systematic uncertainties, in percent, on the ratio of branching fractions.

Source	$\Lambda\eta'(\pi^+\pi^-\gamma)$		$\Lambda\eta'(\pi^+\pi^-\eta)$		$\Lambda\eta(\pi^+\pi^-\pi^0)$	
	L (%)	D (%)	L (%)	D (%)	L (%)	D (%)
$\mathcal{B}(V^0)$	0.73		0.73		0.73	
$\mathcal{B}(\eta^{(\prime)})$	0.0		2.9		2.3	
$f_B/f_{\Lambda_b^0}$	8.0		8.0		8.0	
Fit model	1.7	0.3	1.7	0.3	1.7	0.3
Ratio of ϵ_{acc}	2.0		1.8		1.9	
Ratio of ϵ_{sel}	5.9	5.3	8.6	14.5	7.5	5.9
ϵ_{trig}	1.0		1.0		1.0	
C_γ	–		4.2		4.6	
PID	2.1	0.9	2.0	1.0	2.0	1.0
Multiple Cand	1.4	1.9	2.2	1.4	2.0	1.7
Total	10.6	10.1	13.4	17.5	12.7	11.5

For the average Λ_b^0 pseudorapidity in our signal sample, the ratio $f_B/f_{\Lambda_b^0}$ has a value of 2.5 ± 0.2 .

The systematic uncertainty on the ratio of the branching fractions of the K_s^0 , Λ and $\eta^{(\prime)}$ decays is calculated from the average values from Ref. [20].

There is an uncertainty on the number of signal decays due to the fit model. To evaluate this uncertainty, the parameters that are fixed in the extended unbinned maximum likelihood fit are varied within the uncertainties obtained from the fit to the simulated samples, and the systematic uncertainty is the relative change in the yield obtained from the fit. This is found to be a small effect, 1.7% for the L model and 0.3% for the D model.

The selection efficiencies are calculated with independent simulated samples, produced with different trigger conditions. The uncertainty on the measured ratio of efficiencies is the statistical uncertainty due to the number of simulation events generated. In addition, there is a systematic uncertainty due to the measured efficiency of the trigger selection as the software trigger changed during the data taking in 2012. The early 2012 setup is not modelled in the simulated samples, and so it is assumed that the efficiency of this stage of the trigger selection is the same for both periods. The uncertainty due to this assumption is taken to be 5%, which is consistent with differences in the efficiencies measured in analyses of similar decays. Since this data comprises $\sim 20\%$ of the total data sample, the overall uncertainty on the trigger efficiency is 1%.

The reconstruction efficiency of the photons cannot be determined using the simulated samples, and so a data-driven method is used to correct for this efficiency [42]. The correction factor, C_γ , is found in bins of photon p_T by comparing the relative yields of reconstructed $B^+ \rightarrow J/\psi K^{*+} (\rightarrow K^+\pi^0)$ and $B^+ \rightarrow J/\psi K^+$ decays. Since the $\Lambda_b^0 \rightarrow \Lambda\eta'$ ($\eta' \rightarrow \pi^+\pi^-\gamma$) decay contains the same number of photons as the normalisation channel, this correction cancels in the ratio of efficiencies. However, for the $\Lambda_b^0 \rightarrow \Lambda\eta'$ ($\eta' \rightarrow \pi^+\pi^-\eta$) and

$\Lambda_b^0 \rightarrow \Lambda \eta$ ($\eta \rightarrow \pi^+ \pi^- \pi^0$) decays, there is an extra photon in the signal channel compared to the normalisation channel. The correction factor is therefore applied to these channels, and an uncertainty is introduced due to the limited size of the data sample used to measure it.

The systematic uncertainty of the PID selection is estimated by the difference between the efficiency estimates obtained in data from calibration samples, and the efficiency extracted from the simulation after reweighting the PID variables to match the respective distribution observed in data.

Finally, there is an uncertainty due to the procedure for handling events with more than one candidate. The efficiency for selecting the best candidate using the procedure described earlier, and the fraction of events which contain more than one candidate are both estimated using simulated samples of signal decays. The estimated uncertainty on each of these quantities is around 10%, which is chosen as a conservative uncertainty. This introduces an overall systematic uncertainty of 1.4% to 2.2% depending on the signal channel.

6 Confidence Intervals

The number of signal events observed in each of the signal decays can be used to place a limit on the ratio of branching fractions of the signal decay with respect to the normalisation channel. The unified approach method presented in Ref. [43] is used to place a limit on the branching fraction. This method constructs confidence intervals based on a likelihood ratio method using the probability of observing N_{obs} signal events for a given branching fraction. For this analysis the probability is assumed to follow a Gaussian distribution with a resolution of $\sigma = \sqrt{\sigma_{\text{syst}}^2 + \sigma_{\text{stat}}^2}$, where σ_{syst} is the systematic uncertainty described above and σ_{stat} is the statistical uncertainty on the number of events observed.

The 68% and 90% confidence level (CL) intervals are obtained for the $\Lambda_b^0 \rightarrow \Lambda \eta$ and $\Lambda_b^0 \rightarrow \Lambda \eta'$ decays respectively, by combining the likelihoods of each category. The weighted average of the observed ratio of branching fractions is calculated from the number of events observed in each signal channel with their uncorrelated systematic uncertainties and the values of α in Table 1, and this is used to construct the confidence intervals. The combined L and D categories are used to construct confidence intervals for the $\Lambda_b^0 \rightarrow \Lambda \eta$ decay. The likelihoods from the $\Lambda_b^0 \rightarrow \Lambda \eta'$ ($\eta' \rightarrow \pi^+ \pi^- \gamma$) and $\Lambda_b^0 \rightarrow \Lambda \eta'$ ($\eta' \rightarrow \pi^+ \pi^- \eta$) decays are then combined, with the L and D combined, to give a limit on the branching fraction for the $\Lambda_b^0 \rightarrow \Lambda \eta'$ decay. The limit on the ratio of branching fraction with respect to the normalisation channel is found to be

$$\frac{\mathcal{B}(\Lambda_b^0 \rightarrow \Lambda \eta')}{\mathcal{B}(B^0 \rightarrow K^0 \eta')} < 0.047 \text{ at } 90\% \text{ CL},$$

for the $\Lambda_b^0 \rightarrow \Lambda \eta'$ decay, and for the $\Lambda_b^0 \rightarrow \Lambda \eta$ decay the 68% CL intervals are

$$\frac{\mathcal{B}(\Lambda_b^0 \rightarrow \Lambda \eta)}{\mathcal{B}(B^0 \rightarrow K^0 \eta')} = 0.142_{-0.08}^{+0.11}.$$

Multiplying by the known value of $\mathcal{B}(B^0 \rightarrow K^0\eta')$ gives a limit on the branching fraction of the $\Lambda_b^0 \rightarrow \Lambda\eta'$ decay

$$\mathcal{B}(\Lambda_b^0 \rightarrow \Lambda\eta') < 3.1 \times 10^{-6} \text{ at 90\% CL,}$$

and the 68% CL intervals for the $\Lambda_b^0 \rightarrow \Lambda\eta$ decay are

$$\mathcal{B}(\Lambda_b^0 \rightarrow \Lambda\eta) = (9.3_{-5.3}^{+7.3}) \times 10^{-6}.$$

7 Conclusions

A search is performed for the $\Lambda_b^0 \rightarrow \Lambda\eta'$ and $\Lambda_b^0 \rightarrow \Lambda\eta$ decays in the full dataset recorded by the LHCb experiment during 2011 and 2012, corresponding to an integrated luminosity of 3fb^{-1} . No significant signal is observed above background for the $\Lambda_b^0 \rightarrow \Lambda\eta'$ decay, and some evidence is seen for the $\Lambda_b^0 \rightarrow \Lambda\eta$ at the level of 3σ . The $B^0 \rightarrow K^0\eta'$ decay is used as a normalisation channel, so that a limit is placed on the ratio of $\Lambda_b^0 \rightarrow \Lambda\eta^{(\prime)}$ branching fractions with respect to the $B^0 \rightarrow K^0\eta'$ branching fraction using the unified approach. With the known value of the $B^0 \rightarrow K^0\eta'$ branching fraction, the upper limit on the absolute branching fraction of the $\Lambda_b^0 \rightarrow \Lambda\eta'$ decay is $\mathcal{B}(\Lambda_b^0 \rightarrow \Lambda\eta') < 3.1 \times 10^{-6}$ at 90% CL. The branching fraction of the $\Lambda_b^0 \rightarrow \Lambda\eta$ decay is $\mathcal{B}(\Lambda_b^0 \rightarrow \Lambda\eta) = (9.3_{-5.3}^{+7.3}) \times 10^{-6}$.

These values can be compared with the branching fractions calculated in Ref. [21], and given in Sec. 1. The predicted branching fractions depend strongly on the method used to calculate the hadronic form factors, and on the parameters used in the calculation, as discussed earlier. Our results favour the branching fractions calculated using the pole model to estimate the hadronic form factors. In addition, our results are inconsistent with the prediction for $\mathcal{B}(\Lambda_b^0 \rightarrow \Lambda\eta')$ obtained by neglecting the anomalous contribution to the decay amplitude, indicating that a gluonic component of the η' wavefunction should be present.

Acknowledgements

We express our gratitude to our colleagues in the CERN accelerator departments for the excellent performance of the LHC. We thank the technical and administrative staff at the LHCb institutes. We acknowledge support from CERN and from the national agencies: CAPES, CNPq, FAPERJ and FINEP (Brazil); NSFC (China); CNRS/IN2P3 (France); BMBF, DFG, HGF and MPG (Germany); INFN (Italy); FOM and NWO (The Netherlands); MNiSW and NCN (Poland); MEN/IFA (Romania); MinES and FANO (Russia); MinECo (Spain); SNSF and SER (Switzerland); NASU (Ukraine); STFC (United Kingdom); NSF (USA). The Tier1 computing centres are supported by IN2P3 (France), KIT and BMBF (Germany), INFN (Italy), NWO and SURF (The Netherlands), PIC (Spain), GridPP (United Kingdom). We are indebted to the communities behind the multiple open source software packages on which we depend. We are also thankful for the computing resources and the access to software R&D tools provided by Yandex LLC

(Russia). Individual groups or members have received support from EPLANET, Marie Skłodowska-Curie Actions and ERC (European Union), Conseil général de Haute-Savoie, Labex ENIGMASS and OCEVU, Région Auvergne (France), RFBR (Russia), XuntaGal and GENCAT (Spain), Royal Society and Royal Commission for the Exhibition of 1851 (United Kingdom).

References

- [1] C. Di Donato, G. Ricciardi, and I. Bigi, *$\eta - \eta'$ mixing: from electromagnetic transitions to weak decays of charm and beauty hadrons*, Phys. Rev. **D85** (2012) 013016, [arXiv:1105.3557](#).
- [2] J. L. Rosner, *Quark content of neutral mesons*, Phys. Rev. **D27** (1983) 1101.
- [3] M. R. Ahmady and E. Kou, *A more careful estimate of the charm content of η'* , [arXiv:hep-ph/9903335](#).
- [4] E. V. Shuryak and A. R. Zhitnitsky, *The gluon and charm content of the η' meson and instantons*, Phys. Rev. **D57** (1998) 2001, [arXiv:hep-ph/9706316](#).
- [5] G. Li, Q. Zhao, and C.-H. Chang, *Decays of J/ψ and ψ' into vector and pseudoscalar meson and the pseudoscalar glueball- $q\bar{q}$ mixing*, J. Phys. **G35** (2008) 055002, [arXiv:hep-ph/0701020](#).
- [6] A. Bramon, R. Escribano, and M. D. Scadron, *Mixing of $\eta - \eta'$ mesons in J/ψ decays into a vector and a pseudoscalar meson*, Phys. Lett. **B403** (1997) 339, [arXiv:hep-ph/9703313](#).
- [7] T. Feldmann, P. Kroll, and B. Stech, *Mixing and decay constants of pseudoscalar mesons*, Phys. Rev. **D58** (1998) 114006, [arXiv:hep-ph/9802409](#).
- [8] A. Bramon, R. Escribano, and M. D. Scadron, *The $\eta - \eta'$ mixing angle revisited*, Eur. Phys. J. **C7** (1999) 271, [arXiv:hep-ph/9711229](#).
- [9] F.-G. Cao and A. I. Signal, *Two analytical constraints on the $\eta - \eta'$ mixing*, Phys. Rev. **D60** (1999) 114012, [arXiv:hep-ph/9908481](#).
- [10] A. Bramon, R. Escribano, and M. D. Scadron, *Radiative $VP\gamma$ transitions and $\eta - \eta'$ mixing*, Phys. Lett. **B503** (2001) 271, [arXiv:hep-ph/0012049](#).
- [11] B.-W. Xiao and B.-Q. Ma, *Photon-meson transition form factors of light pseudoscalar mesons*, Phys. Rev. **D71** (2005) 014034, [arXiv:hep-ph/0501160](#).
- [12] R. Escribano and J.-M. Frère, *Study of the $\eta - \eta'$ system in the two mixing angle scheme*, JHEP **06** (2005) 029, [arXiv:hep-ph/0501072](#).

- [13] T. Huang and X.-G. Wu, *Determination of the η – η' mixing angle from the pseudoscalar transition form factors*, Eur. Phys. J. **C50** (2007) 771, [arXiv:hep-ph/0612007](#).
- [14] LHCb collaboration, R. Aaij *et al.*, *Evidence for the decay $B^0 \rightarrow J/\psi\omega$ and measurement of the relative branching fractions of B_s^0 meson decays to $J/\psi\eta$ and $J/\psi\eta'$* , Nucl. Phys. **B867** (2013) 547, [arXiv:1210.2631](#).
- [15] F. Ambrosino *et al.*, *A global fit to determine the pseudoscalar mixing angle and the gluonium content of the η' meson*, JHEP **07** (2009) 105, [arXiv:0906.3819](#).
- [16] R. Escribano and J. Nadal, *On the gluon content of the η and η' mesons*, JHEP **05** (2007) 006, [arXiv:hep-ph/0703187](#).
- [17] R. Escribano, *$J/\psi \rightarrow VP$ decays and the quark and gluon content of the η and η'* , Eur. Phys. J. **C65** (2010) 467, [arXiv:0807.4201](#).
- [18] LHCb collaboration, R. Aaij *et al.*, *Study of η – η' mixing from measurement of $B_{(s)}^0 \rightarrow J/\psi\eta^{(\prime)}$ decay rates*, JHEP **01** (2015) 024, [arXiv:1411.0943](#).
- [19] D. Atwood and A. Soni, *$B \rightarrow \eta' + X$ and the QCD anomaly*, Phys. Lett. **B405** (1997) 150, [arXiv:hep-ph/9704357](#).
- [20] Particle Data Group, K. A. Olive *et al.*, *Review of particle physics*, Chin. Phys. **C38** (2014) 090001.
- [21] M. R. Ahmady, C. S. Kim, S. Oh, and C. Yu, *Heavy baryonic decays of $\Lambda_b \rightarrow \Lambda\eta^{(\prime)}$* , Phys. Lett. **B598** (2004) 203, [arXiv:hep-ph/0305031](#).
- [22] LHCb collaboration, A. A. Alves Jr. *et al.*, *The LHCb detector at the LHC*, JINST **3** (2008) S08005.
- [23] LHCb collaboration, R. Aaij *et al.*, *LHCb detector performance*, Int. J. Mod. Phys. **A30** (2015) 1530022, [arXiv:1412.6352](#).
- [24] R. Aaij *et al.*, *Performance of the LHCb Vertex Locator*, JINST **9** (2014) P09007, [arXiv:1405.7808](#).
- [25] R. Arink *et al.*, *Performance of the LHCb Outer Tracker*, JINST **9** (2014) P01002, [arXiv:1311.3893](#).
- [26] M. Adinolfi *et al.*, *Performance of the LHCb RICH detector at the LHC*, Eur. Phys. J. **C73** (2013) 2431, [arXiv:1211.6759](#).
- [27] A. A. Alves Jr. *et al.*, *Performance of the LHCb muon system*, JINST **8** (2013) P02022, [arXiv:1211.1346](#).
- [28] R. Aaij *et al.*, *The LHCb trigger and its performance in 2011*, JINST **8** (2013) P04022, [arXiv:1211.3055](#).

- [29] V. V. Gligorov and M. Williams, *Efficient, reliable and fast high-level triggering using a bonsai boosted decision tree*, JINST **8** (2013) P02013, [arXiv:1210.6861](#).
- [30] T. Sjöstrand, S. Mrenna, and P. Skands, *A brief introduction to PYTHIA 8.1*, Comput. Phys. Commun. **178** (2008) 852, [arXiv:0710.3820](#).
- [31] I. Belyaev *et al.*, *Handling of the generation of primary events in Gauss, the LHCb simulation framework*, J. Phys. Conf. Ser. **331** (2011) 032047.
- [32] D. J. Lange, *The EvtGen particle decay simulation package*, Nucl. Instrum. Meth. **A462** (2001) 152.
- [33] P. Golonka and Z. Was, *PHOTOS Monte Carlo: A precision tool for QED corrections in Z and W decays*, Eur. Phys. J. **C45** (2006) 97, [arXiv:hep-ph/0506026](#).
- [34] Geant4 collaboration, J. Allison *et al.*, *Geant4 developments and applications*, IEEE Trans. Nucl. Sci. **53** (2006) 270; Geant4 collaboration, S. Agostinelli *et al.*, *Geant4: A simulation toolkit*, Nucl. Instrum. Meth. **A506** (2003) 250.
- [35] M. Clemencic *et al.*, *The LHCb simulation application, Gauss: Design, evolution and experience*, J. Phys. Conf. Ser. **331** (2011) 032023.
- [36] W. D. Hulsbergen, *Decay chain fitting with a Kalman filter*, Nucl. Instrum. Meth. **A552** (2005) 566, [arXiv:physics/0503191](#).
- [37] L. Breiman, J. H. Friedman, R. A. Olshen, and C. J. Stone, *Classification and regression trees*, Wadsworth international group, Belmont, California, USA, 1984.
- [38] B. P. Roe *et al.*, *Boosted decision trees as an alternative to artificial neural networks for particle identification*, Nucl. Instrum. Meth. **A543** (2005) 577, [arXiv:physics/0408124](#).
- [39] G. Punzi, *Sensitivity of searches for new signals and its optimisation*, [arXiv:physics/030863](#).
- [40] T. Skwarnicki, *A study of the radiative cascade transitions between the Upsilon-prime and Upsilon resonances*, PhD thesis, Institute of Nuclear Physics, Krakow, 1986, DESY-F31-86-02.
- [41] LHCb collaboration, R. Aaij *et al.*, *Study of the kinematic dependences of Λ_b^0 production in pp collisions and a measurement of the $\Lambda_b^0 \rightarrow \Lambda_c^+ \pi^-$ branching fraction*, JHEP **08** (2014) 143, [arXiv:1405.6842](#).
- [42] E. Govorkova, *Study of photon reconstruction efficiency using $B^+ \rightarrow J/\psi K^{(*)+}$ decays in the LHCb experiment*, [arXiv:1505.02960](#).
- [43] G. J. Feldman and R. D. Cousins, *A unified approach to the classical statistical analysis of small signals*, Phys. Rev. **D57** (1998) 3873, [arXiv:physics/9711021](#).

LHCb collaboration

R. Aaij³⁸, B. Adeva³⁷, M. Adinolfi⁴⁶, A. Affolder⁵², Z. Ajaltouni⁵, S. Akar⁶, J. Albrecht⁹, F. Alessio³⁸, M. Alexander⁵¹, S. Ali⁴¹, G. Alkhazov³⁰, P. Alvarez Cartelle⁵³, A.A. Alves Jr⁵⁷, S. Amato², S. Amerio²², Y. Amhis⁷, L. An³, L. Anderlini^{17,g}, J. Anderson⁴⁰, M. Andreotti^{16,f}, J.E. Andrews⁵⁸, R.B. Appleby⁵⁴, O. Aquines Gutierrez¹⁰, F. Archilli³⁸, P. d'Argent¹¹, A. Artamonov³⁵, M. Artuso⁵⁹, E. Aslanides⁶, G. Auriemma^{25,n}, M. Baalouch⁵, S. Bachmann¹¹, J.J. Back⁴⁸, A. Badalov³⁶, C. Baesso⁶⁰, W. Baldini^{16,38}, R.J. Barlow⁵⁴, C. Barschel³⁸, S. Barsuk⁷, W. Barter³⁸, V. Batozskaya²⁸, V. Battista³⁹, A. Bay³⁹, L. Beaucourt⁴, J. Beddow⁵¹, F. Bedeschi²³, I. Bediaga¹, L.J. Bel⁴¹, I. Belyaev³¹, E. Ben-Haim⁸, G. Bencivenni¹⁸, S. Benson³⁸, J. Benton⁴⁶, A. Berezhnoy³², R. Bernet⁴⁰, A. Bertolin²², M.-O. Bettler³⁸, M. van Beuzekom⁴¹, A. Bien¹¹, S. Bifani⁴⁵, T. Bird⁵⁴, A. Birnkraut⁹, A. Bizzeti^{17,i}, T. Blake⁴⁸, F. Blanc³⁹, J. Blouw¹⁰, S. Blusk⁵⁹, V. Bocci²⁵, A. Bondar³⁴, N. Bondar^{30,38}, W. Bonivento¹⁵, S. Borghi⁵⁴, M. Borsato⁷, T.J.V. Bowcock⁵², E. Bowen⁴⁰, C. Bozzi¹⁶, S. Braun¹¹, D. Brett⁵⁴, M. Britsch¹⁰, T. Britton⁵⁹, J. Brodzicka⁵⁴, N.H. Brook⁴⁶, A. Bursche⁴⁰, J. Buytaert³⁸, S. Cadeddu¹⁵, R. Calabrese^{16,f}, M. Calvi^{20,k}, M. Calvo Gomez^{36,p}, P. Campana¹⁸, D. Campora Perez³⁸, L. Capriotti⁵⁴, A. Carbone^{14,d}, G. Carboni^{24,l}, R. Cardinale^{19,j}, A. Cardini¹⁵, P. Carniti²⁰, L. Carson⁵⁰, K. Carvalho Akiba^{2,38}, R. Casanova Mohr³⁶, G. Casse⁵², L. Cassina^{20,k}, L. Castillo Garcia³⁸, M. Cattaneo³⁸, Ch. Cauet⁹, G. Cavallero¹⁹, R. Cenci^{23,t}, M. Charles⁸, Ph. Charpentier³⁸, M. Chefdeville⁴, S. Chen⁵⁴, S.-F. Cheung⁵⁵, N. Chiapolini⁴⁰, M. Chrzasczcz⁴⁰, X. Cid Vidal³⁸, G. Ciezarek⁴¹, P.E.L. Clarke⁵⁰, M. Clemencic³⁸, H.V. Cliff⁴⁷, J. Closier³⁸, V. Coco³⁸, J. Cogan⁶, E. Cogneras⁵, V. Cogoni^{15,e}, L. Cojocariu²⁹, G. Collazuol²², P. Collins³⁸, A. Comerma-Montells¹¹, A. Contu^{15,38}, A. Cook⁴⁶, M. Coombes⁴⁶, S. Coquereau⁸, G. Corti³⁸, M. Corvo^{16,f}, B. Couturier³⁸, G.A. Cowan⁵⁰, D.C. Craik⁴⁸, A. Crocombe⁴⁸, M. Cruz Torres⁶⁰, S. Cunliffe⁵³, R. Currie⁵³, C. D'Ambrosio³⁸, J. Dalseno⁴⁶, P.N.Y. David⁴¹, A. Davis⁵⁷, K. De Bruyn⁴¹, S. De Capua⁵⁴, M. De Cian¹¹, J.M. De Miranda¹, L. De Paula², W. De Silva⁵⁷, P. De Simone¹⁸, C.-T. Dean⁵¹, D. Decamp⁴, M. Deckenhoff⁹, L. Del Buono⁸, N. Déléage⁴, D. Derkach⁵⁵, O. Deschamps⁵, F. Dettori³⁸, B. Dey⁴⁰, A. Di Canto³⁸, F. Di Ruscio²⁴, H. Dijkstra³⁸, S. Donleavy⁵², F. Dordei¹¹, M. Dorigo³⁹, A. Dosil Suárez³⁷, D. Dossett⁴⁸, A. Dovbnya⁴³, K. Dreimanic⁵², L. Dufour⁴¹, G. Dujany⁵⁴, F. Dupertuis³⁹, P. Durante³⁸, R. Dzhelyadin³⁵, A. Dziurda²⁶, A. Dzyuba³⁰, S. Easo^{49,38}, U. Egede⁵³, V. Egorychev³¹, S. Eidelman³⁴, S. Eisenhardt⁵⁰, U. Eitschberger⁹, R. Ekelhof⁹, L. Eklund⁵¹, I. El Rifai⁵, Ch. Elsasser⁴⁰, S. Ely⁵⁹, S. Esen¹¹, H.M. Evans⁴⁷, T. Evans⁵⁵, A. Falabella¹⁴, C. Färber¹¹, C. Farinelli⁴¹, N. Farley⁴⁵, S. Farry⁵², R. Fay⁵², D. Ferguson⁵⁰, V. Fernandez Albor³⁷, F. Ferrari¹⁴, F. Ferreira Rodrigues¹, M. Ferro-Luzzi³⁸, S. Filippov³³, M. Fiore^{16,38,f}, M. Fiorini^{16,f}, M. Firlej²⁷, C. Fitzpatrick³⁹, T. Fiutowski²⁷, K. Fohl³⁸, P. Fol⁵³, M. Fontana¹⁰, F. Fontanelli^{19,j}, R. Forty³⁸, O. Francisco², M. Frank³⁸, C. Frei³⁸, M. Frosini¹⁷, J. Fu²¹, E. Furfaro^{24,l}, A. Gallas Torreira³⁷, D. Galli^{14,d}, S. Gallorini^{22,38}, S. Gambetta⁵⁰, M. Gandelman², P. Gandini⁵⁵, Y. Gao³, J. García Pardiñas³⁷, J. Garofoli⁵⁹, J. Garra Tico⁴⁷, L. Garrido³⁶, D. Gascon³⁶, C. Gaspar³⁸, U. Gastaldi¹⁶, R. Gauld⁵⁵, L. Gavardi⁹, G. Gazzoni⁵, A. Geraci^{21,v}, D. Gerick¹¹, E. Gersabeck¹¹, M. Gersabeck⁵⁴, T. Gershon⁴⁸, Ph. Ghez⁴, A. Gianelle²², S. Giani³⁹, V. Gibson⁴⁷, O. G. Girard³⁹, L. Giubega²⁹, V.V. Gligorov³⁸, C. Göbel⁶⁰, D. Golubkov³¹, A. Golutvin^{53,31,38}, A. Gomes^{1,a}, C. Gotti^{20,k}, M. Grabalosa Gándara⁵, R. Graciani Diaz³⁶, L.A. Granado Cardoso³⁸, E. Graugés³⁶, E. Graverini⁴⁰, G. Graziani¹⁷, A. Grecu²⁹, E. Greening⁵⁵, S. Gregson⁴⁷, P. Griffith⁴⁵, L. Grillo¹¹, O. Grünberg⁶³, B. Gui⁵⁹, E. Gushchin³³, Yu. Guz^{35,38}, T. Gys³⁸, C. Hadjivasiliou⁵⁹,

G. Haefeli³⁹, C. Haen³⁸, S.C. Haines⁴⁷, S. Hall⁵³, B. Hamilton⁵⁸, T. Hampson⁴⁶, X. Han¹¹,
 S. Hansmann-Menzemer¹¹, N. Harnew⁵⁵, S.T. Harnew⁴⁶, J. Harrison⁵⁴, J. He³⁸, T. Head³⁹,
 V. Heijne⁴¹, K. Hennessy⁵², P. Henrard⁵, L. Henry⁸, J.A. Hernando Morata³⁷,
 E. van Herwijnen³⁸, M. Heß⁶³, A. Hicheur², D. Hill⁵⁵, M. Hoballah⁵, C. Hombach⁵⁴,
 W. Hulsbergen⁴¹, T. Humair⁵³, N. Hussain⁵⁵, D. Hutchcroft⁵², D. Hynds⁵¹, M. Idzik²⁷,
 P. Ilten⁵⁶, R. Jacobsson³⁸, A. Jaeger¹¹, J. Jalocha⁵⁵, E. Jans⁴¹, A. Jawahery⁵⁸, F. Jing³,
 M. John⁵⁵, D. Johnson³⁸, C.R. Jones⁴⁷, C. Joram³⁸, B. Jost³⁸, N. Jurik⁵⁹, S. Kandybei⁴³,
 W. Kanso⁶, M. Karacson³⁸, T.M. Karbach^{38,†}, S. Karodia⁵¹, M. Kelsey⁵⁹, I.R. Kenyon⁴⁵,
 M. Kenzie³⁸, T. Ketel⁴², B. Khanji^{20,38,k}, C. Khurewathanakul³⁹, S. Klaver⁵⁴,
 K. Klimaszewski²⁸, O. Kochebina⁷, M. Kolpin¹¹, I. Komarov³⁹, R.F. Koopman⁴²,
 P. Koppenburg^{41,38}, M. Korolev³², L. Kravchuk³³, K. Kreplin¹¹, M. Kreps⁴⁸, G. Krocker¹¹,
 P. Krokovny³⁴, F. Kruse⁹, W. Kucewicz^{26,o}, M. Kucharczyk²⁶, V. Kudryavtsev³⁴, A.
 K. Kuonen³⁹, K. Kurek²⁸, T. Kvaratskheliya³¹, V.N. La Thi³⁹, D. Lacarrere³⁸, G. Lafferty⁵⁴,
 A. Lai¹⁵, D. Lambert⁵⁰, R.W. Lambert⁴², G. Lanfranchi¹⁸, C. Langenbruch⁴⁸, B. Langhans³⁸,
 T. Latham⁴⁸, C. Lazzeroni⁴⁵, R. Le Gac⁶, J. van Leerdam⁴¹, J.-P. Lees⁴, R. Lefèvre⁵,
 A. Leflat^{32,38}, J. Lefrançois⁷, O. Leroy⁶, T. Lesiak²⁶, B. Leverington¹¹, Y. Li⁷,
 T. Likhomanenko^{65,64}, M. Liles⁵², R. Lindner³⁸, C. Linn³⁸, F. Lionetto⁴⁰, B. Liu¹⁵, X. Liu³,
 S. Lohn³⁸, I. Longstaff⁵¹, J.H. Lopes², D. Lucchesi^{22,r}, M. Lucio Martinez³⁷, H. Luo⁵⁰,
 A. Lupato²², E. Luppi^{16,f}, O. Lupton⁵⁵, F. Machefert⁷, F. Maciuc²⁹, O. Maev³⁰, K. Maguire⁵⁴,
 S. Malde⁵⁵, A. Malinin⁶⁴, G. Manca⁷, G. Mancinelli⁶, P. Manning⁵⁹, A. Mapelli³⁸, J. Maratas⁵,
 J.F. Marchand⁴, U. Marconi¹⁴, C. Marin Benito³⁶, P. Marino^{23,38,t}, R. Märki³⁹, J. Marks¹¹,
 G. Martellotti²⁵, M. Martinelli³⁹, D. Martinez Santos⁴², F. Martinez Vidal⁶⁶,
 D. Martins Tostes², A. Massafferri¹, R. Matev³⁸, A. Mathad⁴⁸, Z. Mathe³⁸, C. Matteuzzi²⁰,
 K. Matthieu¹¹, A. Mauri⁴⁰, B. Maurin³⁹, A. Mazurov⁴⁵, M. McCann⁵³, J. McCarthy⁴⁵,
 A. McNab⁵⁴, R. McNulty¹², B. Meadows⁵⁷, F. Meier⁹, M. Meissner¹¹, M. Merk⁴¹,
 D.A. Milanese⁶², M.-N. Minard⁴, D.S. Mitzel¹¹, J. Molina Rodriguez⁶⁰, S. Monteil⁵,
 M. Morandin²², P. Morawski²⁷, A. Mordà⁶, M.J. Morello^{23,t}, J. Moron²⁷, A.B. Morris⁵⁰,
 R. Mountain⁵⁹, F. Muheim⁵⁰, J. Müller⁹, K. Müller⁴⁰, V. Müller⁹, M. Mussini¹⁴, B. Muster³⁹,
 P. Naik⁴⁶, T. Nakada³⁹, R. Nandakumar⁴⁹, I. Nasteva², M. Needham⁵⁰, N. Neri²¹, S. Neubert¹¹,
 N. Neufeld³⁸, M. Neuner¹¹, A.D. Nguyen³⁹, T.D. Nguyen³⁹, C. Nguyen-Mau^{39,q}, V. Niess⁵,
 R. Niet⁹, N. Nikitin³², T. Nikodem¹¹, D. Ninci²³, A. Novoselov³⁵, D.P. O’Hanlon⁴⁸,
 A. Oblakowska-Mucha²⁷, V. Obraztsov³⁵, S. Ogilvy⁵¹, O. Okhrimenko⁴⁴, R. Oldeman^{15,e},
 C.J.G. Onderwater⁶⁷, B. Osorio Rodrigues¹, J.M. Otalora Goicochea², A. Otto³⁸, P. Owen⁵³,
 A. Oyanguren⁶⁶, A. Palano^{13,c}, F. Palombo^{21,u}, M. Palutan¹⁸, J. Panman³⁸, A. Papanestis⁴⁹,
 M. Pappagallo⁵¹, L.L. Pappalardo^{16,f}, C. Parkes⁵⁴, G. Passaleva¹⁷, G.D. Patel⁵², M. Patel⁵³,
 C. Patrignani^{19,j}, A. Pearce^{54,49}, A. Pellegrino⁴¹, G. Penso^{25,m}, M. Pepe Altarelli³⁸,
 S. Perazzini^{14,d}, P. Perret⁵, L. Pescatore⁴⁵, K. Petridis⁴⁶, A. Petrolini^{19,j}, M. Petruzzo²¹,
 E. Picatoste Olloqui³⁶, B. Pietrzyk⁴, T. Pilar⁴⁸, D. Pinci²⁵, A. Pistone¹⁹, A. Piucci¹¹,
 S. Playfer⁵⁰, M. Plo Casasus³⁷, T. Poikela³⁸, F. Polci⁸, A. Poluektov^{48,34}, I. Polyakov³¹,
 E. Polcarpo², A. Popov³⁵, D. Popov^{10,38}, B. Popovici²⁹, C. Potterat², E. Price⁴⁶, J.D. Price⁵²,
 J. Prisciandaro³⁹, A. Pritchard⁵², C. Prouve⁴⁶, V. Pugatch⁴⁴, A. Puig Navarro³⁹, G. Punzi^{23,s},
 W. Qian⁴, R. Quagliani^{7,46}, B. Rachwal²⁶, J.H. Rademacker⁴⁶, B. Rakotomiamanana³⁹,
 M. Rama²³, M.S. Rangel², I. Raniuk⁴³, N. Rauschmayr³⁸, G. Raven⁴², F. Redi⁵³, S. Reichert⁵⁴,
 M.M. Reid⁴⁸, A.C. dos Reis¹, S. Ricciardi⁴⁹, S. Richards⁴⁶, M. Rihl³⁸, K. Rinnert⁵²,
 V. Rives Molina³⁶, P. Robbe^{7,38}, A.B. Rodrigues¹, E. Rodrigues⁵⁴, J.A. Rodriguez Lopez⁶²,
 P. Rodriguez Perez⁵⁴, S. Roiser³⁸, V. Romanovsky³⁵, A. Romero Vidal³⁷, M. Rotondo²²,

J. Rouvinet³⁹, T. Ruf³⁸, H. Ruiz³⁶, P. Ruiz Valls⁶⁶, J.J. Saborido Silva³⁷, N. Sagidova³⁰, P. Sail⁵¹, B. Saitta^{15,e}, V. Salustino Guimaraes², C. Sanchez Mayordomo⁶⁶, B. Sanmartin Sedes³⁷, R. Santacesaria²⁵, C. Santamarina Rios³⁷, M. Santimaria¹⁸, E. Santovetti^{24,l}, A. Sarti^{18,m}, C. Satriano^{25,n}, A. Satta²⁴, D.M. Saunders⁴⁶, D. Savrina^{31,32}, M. Schiller³⁸, H. Schindler³⁸, M. Schlupp⁹, M. Schmelling¹⁰, T. Schmelzer⁹, B. Schmidt³⁸, O. Schneider³⁹, A. Schopper³⁸, M. Schubiger³⁹, M.-H. Schune⁷, R. Schwemmer³⁸, B. Sciascia¹⁸, A. Sciubba^{25,m}, A. Semennikov³¹, I. Sepp⁵³, N. Serra⁴⁰, J. Serrano⁶, L. Sestini²², P. Seyfert¹¹, M. Shapkin³⁵, I. Shapoval^{16,43,f}, Y. Shcheglov³⁰, T. Shears⁵², L. Shekhtman³⁴, V. Shevchenko⁶⁴, A. Shires⁹, R. Silva Coutinho⁴⁸, G. Simi²², M. Sirendi⁴⁷, N. Skidmore⁴⁶, I. Skillicorn⁵¹, T. Skwarnicki⁵⁹, E. Smith^{55,49}, E. Smith⁵³, I. T. Smith⁵⁰, J. Smith⁴⁷, M. Smith⁵⁴, H. Snoek⁴¹, M.D. Sokoloff^{57,38}, F.J.P. Soler⁵¹, F. Soomro³⁹, D. Souza⁴⁶, B. Souza De Paula², B. Spaan⁹, P. Spradlin⁵¹, S. Sridharan³⁸, F. Stagni³⁸, M. Stahl¹¹, S. Stahl³⁸, O. Steinkamp⁴⁰, O. Stenyakin³⁵, F. Sterpka⁵⁹, S. Stevenson⁵⁵, S. Stoica²⁹, S. Stone⁵⁹, B. Storaci⁴⁰, S. Stracka^{23,t}, M. Straticiu²⁹, U. Straumann⁴⁰, L. Sun⁵⁷, W. Sutcliffe⁵³, K. Swientek²⁷, S. Swientek⁹, V. Syropoulos⁴², M. Szczekowski²⁸, P. Szczypka^{39,38}, T. Szumlak²⁷, S. T'Jampens⁴, T. Tekampe⁹, M. Teklishyn⁷, G. Tellarini^{16,f}, F. Teubert³⁸, C. Thomas⁵⁵, E. Thomas³⁸, J. van Tilburg⁴¹, V. Tisserand⁴, M. Tobin³⁹, J. Todd⁵⁷, S. Tolk⁴², L. Tomassetti^{16,f}, D. Tonelli³⁸, S. Topp-Joergensen⁵⁵, N. Torr⁵⁵, E. Tournefier⁴, S. Tourneur³⁹, K. Trabelsi³⁹, M.T. Tran³⁹, M. Tresch⁴⁰, A. Trisovic³⁸, A. Tsaregorodtsev⁶, P. Tsopelas⁴¹, N. Tuning^{41,38}, A. Ukleja²⁸, A. Ustyuzhanin^{65,64}, U. Uwer¹¹, C. Vacca^{15,e}, V. Vagnoni¹⁴, G. Valenti¹⁴, A. Vallier⁷, R. Vazquez Gomez¹⁸, P. Vazquez Regueiro³⁷, C. Vázquez Sierra³⁷, S. Vecchi¹⁶, J.J. Velthuis⁴⁶, M. Veltri^{17,h}, G. Veneziano³⁹, M. Vesterinen¹¹, B. Viaud⁷, D. Vieira², M. Vieites Diaz³⁷, X. Vilasis-Cardona^{36,p}, A. Vollhardt⁴⁰, D. Volyanskyy¹⁰, D. Voong⁴⁶, A. Vorobyev³⁰, V. Vorobyev³⁴, C. Voß⁶³, J.A. de Vries⁴¹, R. Waldi⁶³, C. Wallace⁴⁸, R. Wallace¹², J. Walsh²³, S. Wandernoth¹¹, J. Wang⁵⁹, D.R. Ward⁴⁷, N.K. Watson⁴⁵, D. Websdale⁵³, A. Weiden⁴⁰, M. Whitehead⁴⁸, D. Wiedner¹¹, G. Wilkinson^{55,38}, M. Wilkinson⁵⁹, M. Williams³⁸, M.P. Williams⁴⁵, M. Williams⁵⁶, T. Williams⁴⁵, F.F. Wilson⁴⁹, J. Wimberley⁵⁸, J. Wishahi⁹, W. Wislicki²⁸, M. Witek²⁶, G. Wormser⁷, S.A. Wotton⁴⁷, S. Wright⁴⁷, K. Wyllie³⁸, Y. Xie⁶¹, Z. Xu³⁹, Z. Yang³, J. Yu⁶¹, X. Yuan³⁴, O. Yushchenko³⁵, M. Zangoli¹⁴, M. Zavertyaev^{10,b}, L. Zhang³, Y. Zhang³, A. Zhelezov¹¹, A. Zhokhov³¹, L. Zhong³.

¹ Centro Brasileiro de Pesquisas Físicas (CBPF), Rio de Janeiro, Brazil

² Universidade Federal do Rio de Janeiro (UFRJ), Rio de Janeiro, Brazil

³ Center for High Energy Physics, Tsinghua University, Beijing, China

⁴ LAPP, Université Savoie Mont-Blanc, CNRS/IN2P3, Annecy-Le-Vieux, France

⁵ Clermont Université, Université Blaise Pascal, CNRS/IN2P3, LPC, Clermont-Ferrand, France

⁶ CPPM, Aix-Marseille Université, CNRS/IN2P3, Marseille, France

⁷ LAL, Université Paris-Sud, CNRS/IN2P3, Orsay, France

⁸ LPNHE, Université Pierre et Marie Curie, Université Paris Diderot, CNRS/IN2P3, Paris, France

⁹ Fakultät Physik, Technische Universität Dortmund, Dortmund, Germany

¹⁰ Max-Planck-Institut für Kernphysik (MPIK), Heidelberg, Germany

¹¹ Physikalisches Institut, Ruprecht-Karls-Universität Heidelberg, Heidelberg, Germany

¹² School of Physics, University College Dublin, Dublin, Ireland

¹³ Sezione INFN di Bari, Bari, Italy

¹⁴ Sezione INFN di Bologna, Bologna, Italy

¹⁵ Sezione INFN di Cagliari, Cagliari, Italy

¹⁶ Sezione INFN di Ferrara, Ferrara, Italy

¹⁷ Sezione INFN di Firenze, Firenze, Italy

- ¹⁸ *Laboratori Nazionali dell'INFN di Frascati, Frascati, Italy*
- ¹⁹ *Sezione INFN di Genova, Genova, Italy*
- ²⁰ *Sezione INFN di Milano Bicocca, Milano, Italy*
- ²¹ *Sezione INFN di Milano, Milano, Italy*
- ²² *Sezione INFN di Padova, Padova, Italy*
- ²³ *Sezione INFN di Pisa, Pisa, Italy*
- ²⁴ *Sezione INFN di Roma Tor Vergata, Roma, Italy*
- ²⁵ *Sezione INFN di Roma La Sapienza, Roma, Italy*
- ²⁶ *Henryk Niewodniczanski Institute of Nuclear Physics Polish Academy of Sciences, Kraków, Poland*
- ²⁷ *AGH - University of Science and Technology, Faculty of Physics and Applied Computer Science, Kraków, Poland*
- ²⁸ *National Center for Nuclear Research (NCBJ), Warsaw, Poland*
- ²⁹ *Horia Hulubei National Institute of Physics and Nuclear Engineering, Bucharest-Magurele, Romania*
- ³⁰ *Petersburg Nuclear Physics Institute (PNPI), Gatchina, Russia*
- ³¹ *Institute of Theoretical and Experimental Physics (ITEP), Moscow, Russia*
- ³² *Institute of Nuclear Physics, Moscow State University (SINP MSU), Moscow, Russia*
- ³³ *Institute for Nuclear Research of the Russian Academy of Sciences (INR RAN), Moscow, Russia*
- ³⁴ *Budker Institute of Nuclear Physics (SB RAS) and Novosibirsk State University, Novosibirsk, Russia*
- ³⁵ *Institute for High Energy Physics (IHEP), Protvino, Russia*
- ³⁶ *Universitat de Barcelona, Barcelona, Spain*
- ³⁷ *Universidad de Santiago de Compostela, Santiago de Compostela, Spain*
- ³⁸ *European Organization for Nuclear Research (CERN), Geneva, Switzerland*
- ³⁹ *Ecole Polytechnique Fédérale de Lausanne (EPFL), Lausanne, Switzerland*
- ⁴⁰ *Physik-Institut, Universität Zürich, Zürich, Switzerland*
- ⁴¹ *Nikhef National Institute for Subatomic Physics, Amsterdam, The Netherlands*
- ⁴² *Nikhef National Institute for Subatomic Physics and VU University Amsterdam, Amsterdam, The Netherlands*
- ⁴³ *NSC Kharkiv Institute of Physics and Technology (NSC KIPT), Kharkiv, Ukraine*
- ⁴⁴ *Institute for Nuclear Research of the National Academy of Sciences (KINR), Kyiv, Ukraine*
- ⁴⁵ *University of Birmingham, Birmingham, United Kingdom*
- ⁴⁶ *H.H. Wills Physics Laboratory, University of Bristol, Bristol, United Kingdom*
- ⁴⁷ *Cavendish Laboratory, University of Cambridge, Cambridge, United Kingdom*
- ⁴⁸ *Department of Physics, University of Warwick, Coventry, United Kingdom*
- ⁴⁹ *STFC Rutherford Appleton Laboratory, Didcot, United Kingdom*
- ⁵⁰ *School of Physics and Astronomy, University of Edinburgh, Edinburgh, United Kingdom*
- ⁵¹ *School of Physics and Astronomy, University of Glasgow, Glasgow, United Kingdom*
- ⁵² *Oliver Lodge Laboratory, University of Liverpool, Liverpool, United Kingdom*
- ⁵³ *Imperial College London, London, United Kingdom*
- ⁵⁴ *School of Physics and Astronomy, University of Manchester, Manchester, United Kingdom*
- ⁵⁵ *Department of Physics, University of Oxford, Oxford, United Kingdom*
- ⁵⁶ *Massachusetts Institute of Technology, Cambridge, MA, United States*
- ⁵⁷ *University of Cincinnati, Cincinnati, OH, United States*
- ⁵⁸ *University of Maryland, College Park, MD, United States*
- ⁵⁹ *Syracuse University, Syracuse, NY, United States*
- ⁶⁰ *Pontifícia Universidade Católica do Rio de Janeiro (PUC-Rio), Rio de Janeiro, Brazil, associated to ²*
- ⁶¹ *Institute of Particle Physics, Central China Normal University, Wuhan, Hubei, China, associated to ³*
- ⁶² *Departamento de Física, Universidad Nacional de Colombia, Bogota, Colombia, associated to ⁸*
- ⁶³ *Institut für Physik, Universität Rostock, Rostock, Germany, associated to ¹¹*
- ⁶⁴ *National Research Centre Kurchatov Institute, Moscow, Russia, associated to ³¹*
- ⁶⁵ *Yandex School of Data Analysis, Moscow, Russia, associated to ³¹*
- ⁶⁶ *Instituto de Física Corpuscular (IFIC), Universitat de Valencia-CSIC, Valencia, Spain, associated to ³⁶*
- ⁶⁷ *Van Swinderen Institute, University of Groningen, Groningen, The Netherlands, associated to ⁴¹*

- ^a *Universidade Federal do Triângulo Mineiro (UFMT), Uberaba-MG, Brazil*
- ^b *P.N. Lebedev Physical Institute, Russian Academy of Science (LPI RAS), Moscow, Russia*
- ^c *Università di Bari, Bari, Italy*
- ^d *Università di Bologna, Bologna, Italy*
- ^e *Università di Cagliari, Cagliari, Italy*
- ^f *Università di Ferrara, Ferrara, Italy*
- ^g *Università di Firenze, Firenze, Italy*
- ^h *Università di Urbino, Urbino, Italy*
- ⁱ *Università di Modena e Reggio Emilia, Modena, Italy*
- ^j *Università di Genova, Genova, Italy*
- ^k *Università di Milano Bicocca, Milano, Italy*
- ^l *Università di Roma Tor Vergata, Roma, Italy*
- ^m *Università di Roma La Sapienza, Roma, Italy*
- ⁿ *Università della Basilicata, Potenza, Italy*
- ^o *AGH - University of Science and Technology, Faculty of Computer Science, Electronics and Telecommunications, Kraków, Poland*
- ^p *LIFAELS, La Salle, Universitat Ramon Llull, Barcelona, Spain*
- ^q *Hanoi University of Science, Hanoi, Viet Nam*
- ^r *Università di Padova, Padova, Italy*
- ^s *Università di Pisa, Pisa, Italy*
- ^t *Scuola Normale Superiore, Pisa, Italy*
- ^u *Università degli Studi di Milano, Milano, Italy*
- ^v *Politecnico di Milano, Milano, Italy*
- [†] *Deceased*